Journal of Solid State Chemistry **160,** 340–349 (2001)
doi:10.1006/jssc.2000.9238, available online at http://www.idealibrary.com on IDEAL®

# Crystal Structure of Calcium-Deficient Carbonated Hydroxyapatite. Thermal Decomposition

T. I. Ivanova,* O. V. Frank-Kamenetskaya,* A. B. Kol'tsov,* and V. L. Ugolkov†

*Department of Crystallography, Saint Petersburg State University, St. Petersburg, Russia; and †Institute for Problems of Mechanical Engineering, St. Petersburg, Russia
E-mail: tatjana@ik2494.spb.edu

Received December 21, 2000; in revised form April 26, 2001; accepted May 11, 2001; published online July 16, 2001

**Full Rietveld refinement of the crystal structure of the synthetic calcium-deficient carbonated apatite $Ca1_{3.40}[Ca2_{5.90}(NH_4)_{0.10}][(PO_4)_{4.95}(CO_3)_{1.05}(H_2O)_{0.30}][(OH)_{1.65}(H_2O)_{0.45}]$ (space group $P6_3/m$; $a = 9.437(1)$, $c = 6.888(1)$ Å; $Z = 1$; $R_{wp} = 5.23\%$) was carried out using X-ray powder diffraction data. The use of the model with the split position of O3 atom made it possible to find two orientations of $CO_3$ triangles sharing one of their edges. They occupy randomly the adjacent faces of a $PO_4$ tetrahedron that are parallel to the *c* axis. O3c atoms coordinating carbon atoms are shifted by 0.37 Å from O3p atoms belonging to $PO_4$ tetrahedra. The charge unbalance occurring when $[CO_3]^{2-}$ ions replace $[PO_4]^{3-}$ groups is primarily compensated by vacancies in Ca1 sites. The studies of the sample thermal decomposition performed by simultaneous thermal analysis and by X-ray diffraction helped to analyze the localization and the amount of lattice water that enhanced the reliability of the structural model.** © 2001 Academic Press

*Key Words:* **carbonated apatite; crystal structure; X-ray powder diffraction; Rietveld refinement; thermal decomposition.**

## INTRODUCTION

Nonstoichiometric carbonated apatites are the main mineral components of human and animal hard tissues (bones and teeth). They are increasingly used as biocompatible materials for medical purposes. The basic structure of apatite $Ca_5(PO_4)_3(OH, F, Cl)$ was determined in 1930 (1). It can be described (Fig. 1) as the three-dimensional network of $PO_4$ tetrahedra, which are linked together by the columns of ninefold coordinated Ca1 atoms (Fig. 2a). The channels passing through the network have the axes coinciding with the sixfold screw axes and contain the triangles of sevenfold coordinated Ca2 atoms (Fig. 2b) and $OH^-$, $F^-$, or $Cl^-$ ions.

The crystal structure of carbonated apatite still remains subject to uncertainties since the exact location of carbonate ions have not yet been determined directly from the diffraction data. Besides, the numerous possibilities of compensation of charge unbalance occurring when $CO_3$ ions enter the apatite structure have not been fully clarified.

The principal point complicating the situation is that crystallites of carbonated apatites are too small for single-crystal structure determinations. The only successful attempt to obtain large single crystals of carbonated apatite was reported in (2). The hydrothermally grown needle crystals of 3–12 mm in length had extremely low $CO_2$ content (from 0.09 to 0.65 wt%). A number of Rietveld refinements from powder diffraction data has been made (3–6) for carbonated apatites, however, without any success in the localization of the carbonate ions in the structure. This failure seems to be related to the low carbonate content and poor crystallinity of the samples (for example, enamel apatites) as well as to the restrictions imposed by the authors on the structural models. No attempt has been made up to now to determine the position and the number of $CO_3$ ions per unit cell in the process of structural refinement. However, some evidence of the partial replacement of $PO_4$ tetrahedra by $CO_3$ triangles was found (4–6) in the diminution of the occupancies of phosphorus sites (from 0.93 to 0.79) and in the changes in P–O bond lengths in the tetrahedra (Table 1).

In general, two types (A and B) of carbonated apatites are distinguished (7), taking into account the data of infrared (IR) absorption spectroscopic studies, of chemical analyses, and of the changes in their lattice constants in comparison with fluor- and hydroxyapatites. A-type carbonated apatites have increased lattice constants *a* with $CO_3$ ions substituting for OH groups in the channels. Carbonated apatites of B type are usually characterized by reduced *a* lattice constants resulting from the substitutions of $PO_4$ tetrahedra by smaller $CO_3$ triangles. However, many of the B-type apatites have somewhat increased lattice constants *a* mainly due to the substitutions of vacancies in the channel, oxygen tetrahedral, and, probably, calcium sites by water molecules. The vacancies balance the deficiency of negative charge when $[CO_3]^{2-}$ ions replace $[PO_4]^{3-}$ groups. There



0022-4596/01 $35.00

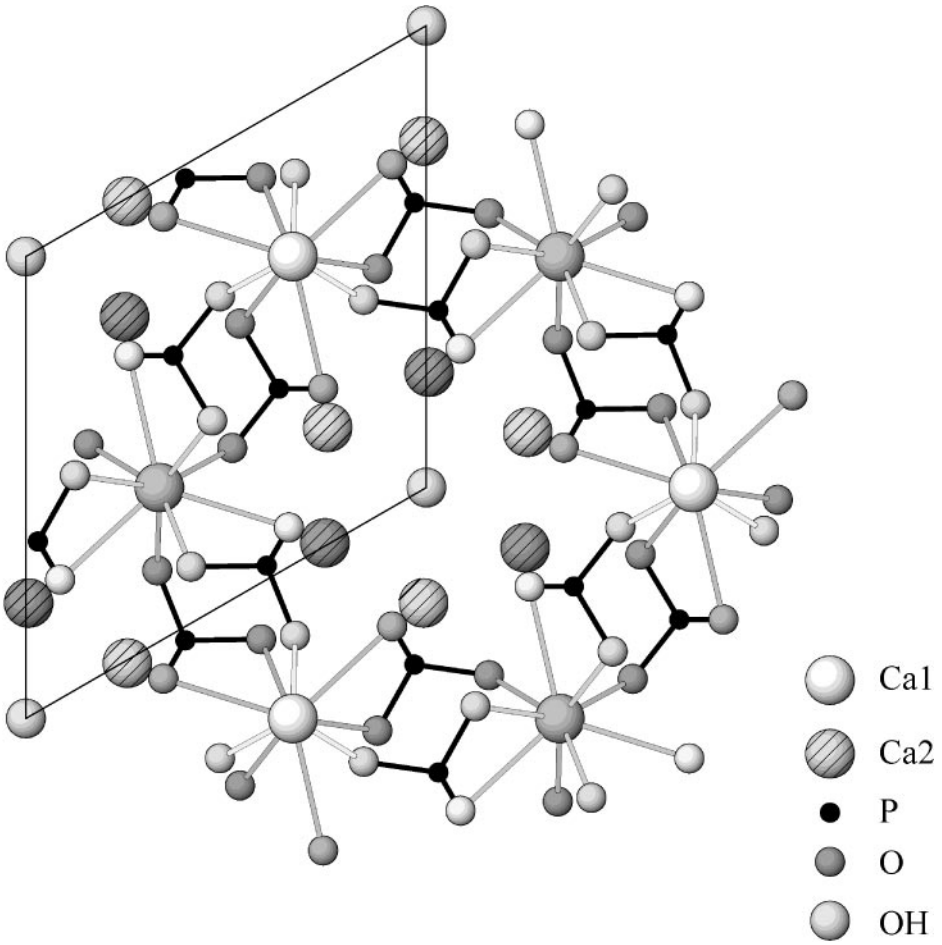


**FIG. 1.** Crystal structure of apatite. Projection onto the (0001) plane.

are also apatites with $CO_3$ ions in both the channel and tetrahedral sites (8).

Polarized IR spectroscopy data (7) show the planes of $CO_3$ triangles to be nearly parallel to the $c$ axis when substituting for OH groups in the channels. When in $PO_4$ sites, $CO_3$ triangles have their planes oblique to the $c$ axis, making an angle of $37 \pm 4^\circ$ to it, and are thought to occupy the sloping faces of the tetrahedra. Thus it seems that three oxygen atoms O1, O2, and O3 of the tetrahedra form the coordination for the carbon atoms.

Thermal expansion of hydroxyapatite lattice between 20 and 600°C is linear with $\Delta a/a = 12.2\text{–}14.8 \times 10^{-6}$ and $\Delta c/c = 11.1\text{–}12.7 \times 10^{-6}$ per °C (9–11). The thermal decomposition of carbonated apatites as summarized in (7) has the following common features. Well-crystallized synthetic apatites lose surface-bound water up to $\sim$120°C and lattice water up to 400–500°C. The latter loss is accompanied by a decrease of $\sim$0.02 Å in the lattice constant $a$ for sodium-containing carbonated apatites and a much smaller contraction ($\sim$0.003 Å) in the absence of $Na^+$ ions. Carbonate loss in air generally starts at 550°C and is usually complete at 900 to 1000°C, depending on the time and composition. On heating B-type carbonated apatites at temperatures from 480 to 800°C the changes in the location of $CO_3$ ions occur: some part of them move from $PO_4$ to OH sites. This is accompanied by a small ($\sim$0.1 Å) increase in the value of lattice constant $a$ and by the appearance of the IR bands from $CO_3^{2-}$ replacing $OH^-$ ions. The number of carbonate ions in the channel sites is thought to be limited by the number of hydroxyl ions in these positions before heating. Carbonate loss is usually followed by the formation of CaO (and $Na_2O$ if sodium is present) and hydroxyapatite. If the Ca/P molar ratio is less than 1.667 ("ideal" Ca/P ratio in stoichiometric hydroxyapatite), whitlockite $Ca_3(PO_4)_2$ may also be present. Well-crystallized carbonated apatites do not contain pyrophosphate after heating, which is probably due to the absence of $HPO_4^{2-}$ ions in the unheated apatite.

The main aim of the present work is to carry out a full Rietveld refinement of the crystal structure of the synthetic calcium-deficient carbonated apatite of B-type including the

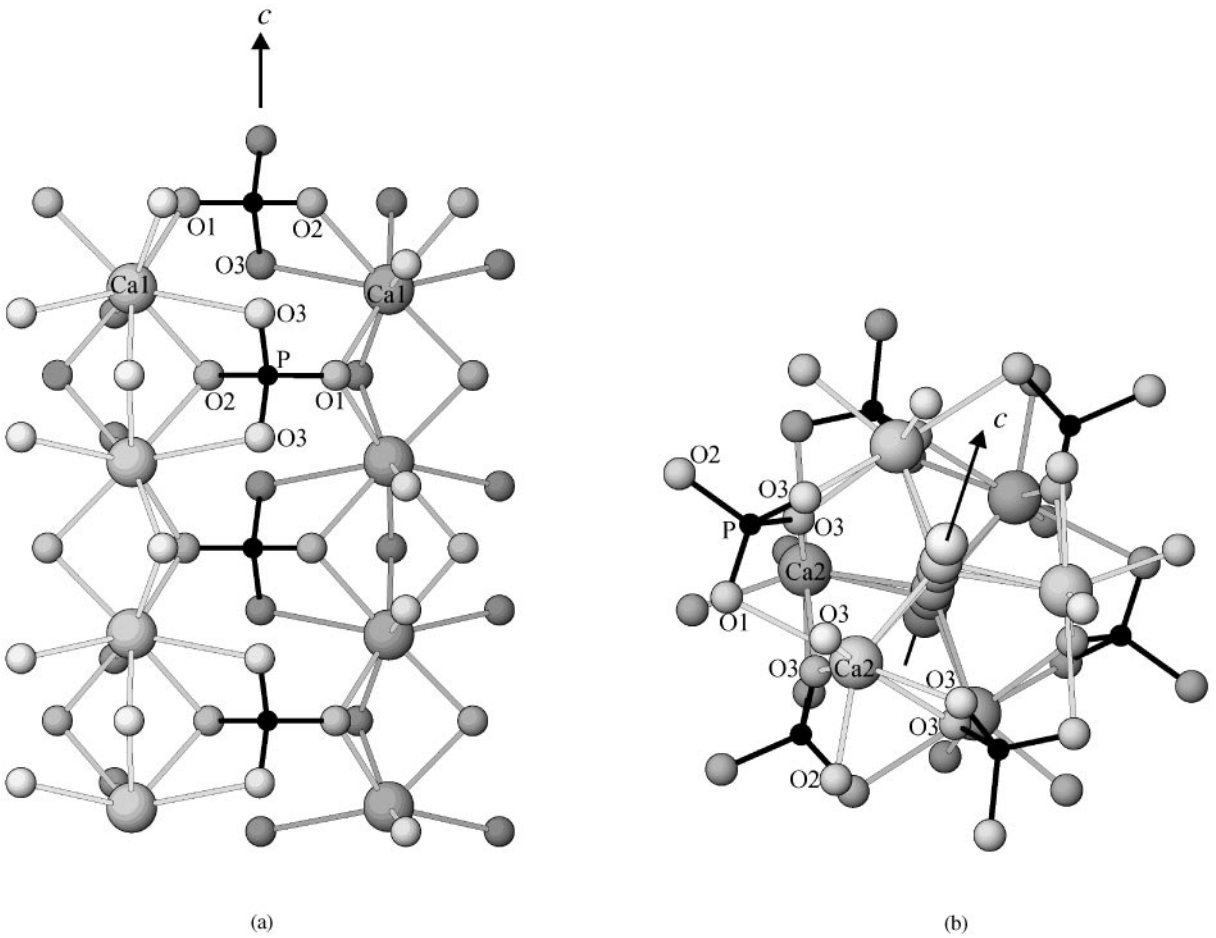


**FIG. 2.** Types of calcium polyhedra in the structure of apatite. (a) Columns of ninefold coordinated Ca1 polyhedra, and (b) triangles of sevenfold coordinated Ca2 polyhedra.

localization of the $CO_3$ groups. Besides, changes in the lattice constants of apatite and its phase transformations at elevated temperatures were studied by simultaneous thermal analysis and by X-ray diffraction. Presenting a separate scientific interest these data helped to analyze the localization and amount of lattice water that enhanced the reliability of the structural model.

## EXPERIMENTAL

### *Sample*

The well-crystallized powder of a single-phase hydroxyapatite with high carbonate content was prepared by the reaction of $CaCO_3$ (calcite) with $NH_4H_2PO_4$ solution under hydrothermal conditions. Fine calcite powder was treated with 0.2 M $NH_4H_2PO_4$ solution in a stainless steel autoclave at 250°C and 1 kbar for 10 days. A minor amount of 2 M $NH_4OH$ was added to the starting solution to bring the pH value to 9. The reaction product of white color with a grain size of about 10 μm was washed with distilled water and then dried in air. The chemical composition of the prepared hydroxyapatite sample was (in wt%) CaO, 54.56; $P_2O_5$, 5.71; $CO_2$, 4.40 and $NH_4$, 0.20. These data were obtained by microprobe analysis (Ca, P) using Camscan-4 (the analyst, Yu. L. Kretser) and by the gas-volumetric method (C, N) at 1100°C in an oxygen current (the analyst, S. N. Zimina). The lattice constants of the sample were found to be $a = 9.437(1)$ and $c = 6.888(1)$ Å, which are close to those of human tooth enamel apatite. IR spectrum showed bands at 880, 1420, and 1460 $cm^{-1}$, which could be assigned to $CO_3$ ions replacing $PO_4$ tetrahedra. A weak diffused band occurring between 1640 and 1660 $cm^{-1}$ could be assigned to molecular water accumulated in the structure. Thus, the chemical formula of the sample can be presented as $Ca_{9.50}(NH_4)_{0.10}(PO_4)_{5.05}(CO_3)_{0.95}(OH)_2$, accounting for the complete filling of channel sites with OH groups.

**TABLE 1**
**Distances (in Å) and Angles (in °) in $PO_4$ Tetrahedra in the Crystal Structures of Natural and Synthetic B-Type Carbonated Apatites and of Stoichiometric Hydroxyapatite**

| Sample(s) | Tooth enamel of *Cervus elaphus* (5) | | Human tooth enamel[a] (6) | Synthetic hydroxyapatite (sample H6G) (6) | Natural francolite (4) | Synthetic hydroxyapatite (our data) | | Holly Springs hydroxyapatite (13) |
|---|---|---|---|---|---|---|---|---|
| | Modern | Oldest fossil | | | | Model 1 | Model 2 | |
| $CO_2$ (wt%) | 3.03 | 3.55 | 2.82 | 3.15 | 4.80 | 4.40 | | none |
| Occupations | | | | | | | | |
| P | 0.894(10) | 0.884(10) | 0.922 (± 0.025)[b] | 0.931(5) | 0.788(18) | 0.842(6) | 0.824(3) | 1.0 |
| O1 | 1.12(2) | 1.08(2) | 0.913 (± 0.010) | 1.020(7) | 0.902(28) | 0.996(5) | 0.932(5) | 1.0 |
| O2 | 1.04(2) | 1.04(18) | 0.973 (± 0.012) | 1.013(8) | 0.986(24) | 0.978(6) | 0.945(5) | 1.0 |
| O3 | 1.0 | 1.0 | 0.903 (± 0.027) | 1.007(7) | 1.0 | 1.020(12) | 1.019(9)[c] | 1.0 |
| Distances | | | | | | | | |
| P–O1 | 1.515(1) | 1.512(1) | 1.545 (± 0.022) | 1.528(6) | 1.468 | 1.534(5) | 1.536(3) | 1.537 |
| P–O2 | 1.561(1) | 1.579(1) | 1.460 (± 0.024) | 1.481(5) | 1.483 | 1.539(5) | 1.543(3) | 1.545 |
| P–O3 × 2 | 1.500(1) | 1.476(1) | 1.531 (± 0.017) | 1.532(4) | 1.548 | 1.500(4) | 1.556(3) | 1.529 |
| P–O mean | 1.519 | 1.511 | 1.517 | 1.518 | 1.512 | 1.518 | 1.548 | 1.535 |
| Angles | | | | | | | | |
| O1–P–O2 | 108.4 | 107.1 | 111.4 | 110.6 | 112.0 | 111.0(1) | 110.6(1) | 111.1 |
| O1–P–O3 | 109.9 | 110.1 | 111.1 | 111.3 | 110.4 | 110.5(1) | 109.9(1) | 111.4 |
| O2–P–O3 | 108.0 | 108.2 | 107.9 | 107.7 | 107.3 | 106.9(1) | 108.4(1) | 107.5 |
| O3–P–O3 | 112.4 | 113.0 | 107.1 | 108.3 | 109.4 | 111.0(2) | 108.9(2) | 107.8 |
| O–P–O mean | 109.7 | 109.6 | 109.4 | 109.5 | 109.8 | 109.9 | 109.5 | 109.5 |

[a] Means and standard deviations calculated for 12 samples.
[b] Calculated from the numbers of P, O1, O2, and O3 atoms per unit cell available in the original paper.
[c] Sum of (O3p + O3c) occupancies.

*Simultaneous Thermal Analysis*

STA was performed on Netzsch STA 429 facility with a conventional Pt–Pt/Rh sample holder capable of simultaneous recording of thermogravimetric (TG), derivative thermogravimetric (DTG), and differential scanning calorimetric (DSC) curves in the temperature range of 20–1400°C. The measurements of the powder sample (30 mg) were done under ambient pressure and at a heating rate of 10°C/min from 60 to 1000°C. TG and DTG curves of the studied sample are presented in Fig. 3a.

*X-Ray Powder Diffraction Studies*

*Data collection.* Diffraction pattern of the polycrystalline sample was measured using a conventional powder autodiffractometer with Bragg–Brentano geometry and a graphite monochromator placed on the diffracted beam. Cu$K\alpha$-radiation was used. The powder spectrum was recorded at 25°C in the range of $2\theta = 9°$–$120°$ with a step of $0.02° 2\theta$ and a counting time of 80 s per data point. A 2-mm source slit and a 0.25-mm receiving slit were placed.

To study lattice deformations and phase transformations of the sample with temperature the high-temperature KRV camera was installed on the diffractometer. Powder spectra were collected in the temperature range of 25°–750°C with a step of 25 or 50°C. The range of data collection was $2\theta = 25°$–$55°$. The unit cell constants were refined from the $2\theta$ positions of 15 reflections by the least-squares method with the accuracy of 0.01–0.02%. Dependencies $a$, $c(T)$ are shown in Fig. 3b.

*Structure refinement.* Rietveld refinement of the crystal structure of carbonated hydroxyapatite was carried out using the RIETICA program package (12). The absorption correction for a flat sample was used. The LP factor was also accounted for. At the first step $2\theta$ zero point, unit cell constants were refined together with the simulation of the background and peak shape using, respectively, fifth-order polynomial and asymmetric pseudo-Voigt functions. A preferred orientation along [001] was taken into account with the Marsh model.

No evident violations of hexagonal symmetry were found on the X-ray diffraction pattern of the sample. Therefore, the refinement of the structure was carried out in the space group $P6_3/m$. The atomic positional parameters of the structure of the Holly Springs hydroxyapatite single crystal

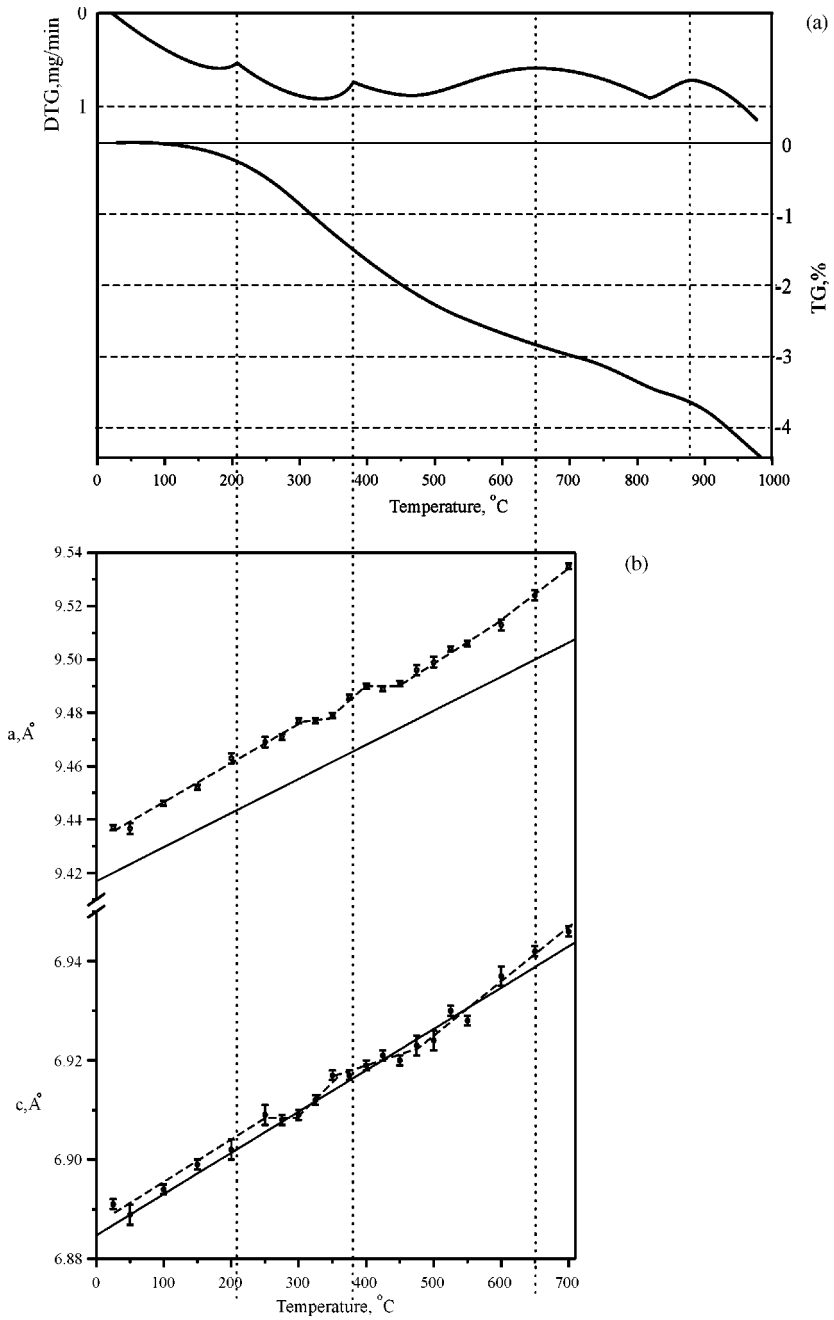


**FIG. 3.** (a) TG and DTG curves showing, respectively, the weight loss of the sample (in %) and its rate (in mg per min). (b) The changes of lattice dimensions of the sample at elevated temperatures. Dots with error bars and dashed lines represent the experimental data, solid lines the data (9–11) on the thermal expansion of the stoichiometric hydroxyapatite lattice. See text for further explanations.

(13) (Table 2) were taken as the starting point of the refinement. The atomic coordinates, the occupancies of the crystallographic positions, and the thermal parameters were then refined, the last ones in anisotropic approximation. The refinement of 20 structural parameters using a set of 290 reflections converged to the following conventional $R$ values: $R_p = 5.63\%$, $R_{wp} = 6.41\%$, and $R_{exp} = 5.97\%$. The final positional and thermal atomic parameters together with the occupancies of the basic crystallographic positions are listed in Table 2 (model 1). Shortened P–O3 distances of 1.500 Å in comparison with the other P–O distances in a tetrahedron (Table 1) and implausibly low-temperature factors of O3 atoms were thought to indicate the untrue position of O3 atoms.

Therefore, the O3 atom was excluded from the model, and Fourier difference map was then built. Two peaks with unequal intensity were found on the map in the locality of the O3 atom—at (0.34, 0.26, 0.07), exhibiting higher intensity, and at (0.36, 0.30, 0.09), which was much weaker. At the next step model 2 was established with the position of the O3 atom split into two (O3p and O3c) with the coordinates taken as they appeared in the Fourier difference map and then refined together. The refinement improved the temperature factors and led to a reasonable P–O3p distance of 1.556 Å and to equal O1–O3c, O2–O3c, and O3c–O3c distances of 2.22 Å (model 2 in Table 2). This value is exactly the same as in $CO_3$ triangles in the structure of calcite (14). This made it possible to fix two carbon atoms C1 and C2 (Table 2) at $z = \frac{1}{4}$ in the centers of the triangles O1–O3c–O3c and O2–O3c–O3c, respectively, at the equal distances of 1.282 Å from each of the oxygen atoms (Fig. 4). A final refinement of 29 structural parameters of the model using the same set of reflections gave a somewhat better fit to the experimental data (Fig. 5) with the following $R$ values: $R_p = 4.85\%$, $R_{wp} = 5.23\%$, and $R_{exp} = 5.05\%$. All the thermal parameters except those for carbon atoms were refined in anisotropic approximation. The final structural data for model 2 are listed in Tables 1 and 2.

## RESULTS AND DISCUSSION

### *Thermal Decomposition*

Five regions of the weight loss can be distinguished on the DTG curve (upper curve in Fig. 3a):

(i) between 60 and 210°C with the loss of 0.3% from the initial sample weight of 30 mg;

(ii) between 210 and 375°C with the weight loss of 1.1%;

(iii) between 375 and 650°C with the weight loss of 1.4%;

(iv) between 650 and 870°C with the weight loss of 0.8%;

(v) starting at 870 and gaining to 980°C with the weight loss of 0.6%.

The total weight loss on heating from 60 to 980°C is evaluated to be about 4.3%.

**TABLE 2**
**Positional and Thermal Atomic Parameters of the Crystal Structures of Synthetic Carbonated and Stoichiometric Hydroxyapatites (Space Group $P6_3/m$)**

| | $Ca_{9.50}(NH_4)_{0.10}(PO_4)_{5.05}(CO_3)_{0.95}(OH)_2$ (our data) | | Sample H6G with 3.15 wt% of $CO_2$ (6) | Holly springs hydroxyapatite $Ca_{10}(PO_4)_6(OH)_2$ (13) |
|---|---|---|---|---|
| | Model 1 | Model 2 | | |
| Radiation | X-rays (Cu$K\alpha$) | X-rays (Cu$K\alpha$) | X-rays (Cu$K\alpha$) | Neutrons |
| Method | Rietveld refinement | Rietveld refinement | Rietveld refinement | Single-crystal refinement |
| R-value (%) | $R_{wp} = 6.41$ | $R_{wp} = 5.23$ | $R_{wp} = 8.1$ | $R_F = 2.3$ |
| Lattice constants (Å) | | | | |
| $a$ | 9.4372(6) | | 9.4394(4) | 9.424(4) |
| $c$ | 6.8881(2) | | 6.8861(3) | 6.879(4) |
| $D_x$ (g/cm$^3$) | 2.990 | 2.997 | 3.120 | 3.165 |
| | Positional and thermal atomic parameters | | | |
| Ca1 4f $\frac{1}{3}\ \frac{2}{3}\ z$ | | | | |
| $z$ | 0.0058(4) | 0.0011(3) | 0.0021(4) | 0.0013(1) |
| $B_{iso}$ (Å$^2$) | 2.11(4) | 1.75(3) | —[a] | 0.42(4)[b] |
| Occupancy | 0.837(2) | 0.848(2) | 1.0 | 1.0 |
| Ca2 6h $xy\ \frac{1}{4}$ | | | | |
| $x$ | 0.2508(2) | 0.2457(2) | 0.2478(2) | 0.2465(1) |
| $y$ | 0.9921(3) | 0.9879(2) | 0.9917(3) | 0.9931(1) |
| $B_{iso}$ (Å$^2$) | 1.09(2) | 0.67(2) | | 0.38(4) |
| Occupancy | 1.008(2) | 0.985(2) | 0.978(4) | 1.0 |
| P 6h $xy\ \frac{1}{4}$ | | | | |
| $x$ | 0.4031(3) | 0.3991(3) | 0.3995(3) | 0.3983(1) |
| $y$ | 0.3734(3) | 0.3692(3) | 0.3691(3) | 0.3683(1) |
| $B_{iso}$ (Å$^2$) | 0.06(4) | 0.15(3) | | 0.24(3) |
| Occupancy | 0.842(6) | 0.824(3) | 0.931(5) | 1.0 |
| O1 6h $xy\ \frac{1}{4}$ | | | | |
| $x$ | 0.3335(6) | 0.3264(5) | 0.3319(6) | 0.3282(2) |
| $y$ | 0.4896(6) | 0.4829(5) | 0.4862(6) | 0.4846(1) |
| $B_{iso}$ (Å$^2$) | 0.96(16) | 0.34(13) | | 0.52(5) |
| Occupancy | 0.966(5) | 0.932(5) | 1.020(7) | 1.0 |

**TABLE 2**—*Continued*

| | $Ca_{9.50}(NH_4)_{0.10}(PO_4)_{5.05}(CO_3)_{0.95}(OH)_2$ (our data) | | | Sample H6G with 3.15 wt% of $CO_2$ (6) | Holly springs hydroxyapatite $Ca_{10}(PO_4)_6(OH)_2$ (13) | |
|---|---|---|---|---|---|---|
| | Model 1 | Model 2 | | | | |
| O2 6h $xy\frac{1}{4}$ | | | | | | |
| $x$ | 0.5913(6) | 0.5879(6) | | 0.5806(7) | 0.5876(1) | |
| $y$ | 0.4696(6) | 0.4695(6) | | 0.4614(7) | 0.4652(1) | |
| $B_{iso}$ (Å$^2$) | 1.39(13) | 0.32(9) | | | 0.84(6) | |
| Occupancy | 0.978(6) | 0.945(5) | | 1.013(8) | 1.0 | |
| O3 12i $xyz$ | | O3p | O3c | | | |
| $x$ | 0.3510(5) | 0.3409(4) | 0.362(4) | 0.3437(5) | 0.3433(1) | |
| $y$ | 0.2694(5) | 0.2579(4) | 0.299(4) | 0.2597(5) | 0.2579(1) | |
| $z$ | 0.0705(6) | 0.0668(4) | 0.089(4) | 0.0697(5) | 0.0704(1) | |
| $B_{iso}$ (Å$^2$) | 0.07(9) | 0.64(4) | 2.4(4) | | 0.98(8) | |
| Occupancy | 1.020(12) | 0.832(9) | 0.187(9) | 1.007(7) | 1.0 | |
| $O_H$ 4e 00$z$ | | | | | O | H |
| $z$ | 0.1692(18) | 0.1884(17) | | 0.1906(22) | 0.1978(7) | 0.0608(14) |
| $B_{iso}$ (Å$^2$) | 9.8(5) | 11.6(3) | | | 1.05(10) | |
| Occupancy | 0.557(4) | 0.602(4) | | 0.518(10) | 0.5 | 0.5 |
| C1 6h $xy\frac{1}{4}$ | | | | | | |
| $x$ | | 0.3522 | | | | |
| $y$ | | 0.3618 | | | | |
| $B_{iso}$ (Å$^2$) | | 3(2) | | | | |
| Occupancy | | 0.09(1) | | | | |
| C2 6h $xy\frac{1}{4}$ | Not included | | | Not included | Not included | |
| $x$ | into the refinement | 0.4380 | | into the refinement | into the refinement | |
| $y$ | | 0.3550 | | | | |
| $B_{iso}$ (Å$^2$) | | 3(2) | | | | |
| Occupancy | | 0.09(1) | | | | |

[a] Thermal factors are not available in the original paper.
[b] Isotropic thermal factors were calculated from the anisotropic values of $\beta_{ij}$ available in the original paper.

Four plateaus are clearly distinguished in the plots showing the changes in unit cell dimensions of the sample with temperature (Fig. 3b). Two of them (at 300–350°C and at 400–450°C) break the monotonous increase of the constant $a$ with temperature and two (at 250–300°C and at 350–450°C) of the constant $c$. At 750°C phase transformation occurred with the formation of another calcium phosphate—whitlockite $Ca_3(PO_4)_2$.

Considering the thermal expansion curves of stoichiometric hydroxyapatite, which are shown for comparison in the same figure, it is easy to estimate the local lattice diminutions and enlargements of the carbonated sample studied. The plateau between 250 and 300°C marks the reduction of lattice constant $c$ by 0.005 Å, whereas that one between 300 and 300°C reflects the reduction of lattice constant $a$ by 0.007 Å. These plateaus together are associated with the weight loss of $\sim$1.1% (see the second of the above indicated regions on the DTG curve) and, thus, can be assigned to the removal of two different types of structural water. The plateau between 350 and 450°C with the reduction of lattice constant $c$ by 0.008 Å can most probably be assigned to the relocation of carbonate ions from tetrahedral to channel sites with their partial loss as $CO_2$ molecules (the third of the above indicated regions on the DTG curve associated with the weight loss of 1.4%). Both of these processes might cause the slight expansion of lattice constant $a$ by 0.004 Å between 350 and 400°C, which is followed by its reduction by the same 0.004 Å between 400 and 450°C. The latter might be the consequence of carbonate removal from the channel sites. The fourth region of the weight loss marked on the DTG curve may be associated with the carbonate loss from tetrahedral sites and is in accord with the continual enlargement of lattice constant $a$ by 0.018 Å between 600 and 750°C. The fifth of the above indicated regions on the DTG curve associated with the weight loss of 0.6% can be assigned to the next stage of sample decarbonation. Mean relative changes of the sample lattice constants (due to thermal expansion as well as to dehydration and decarbonation) between 20 and 750°C in the [100] and [001] directions are estimated to be, respectively, $\Delta a/a = 16.8 \times$

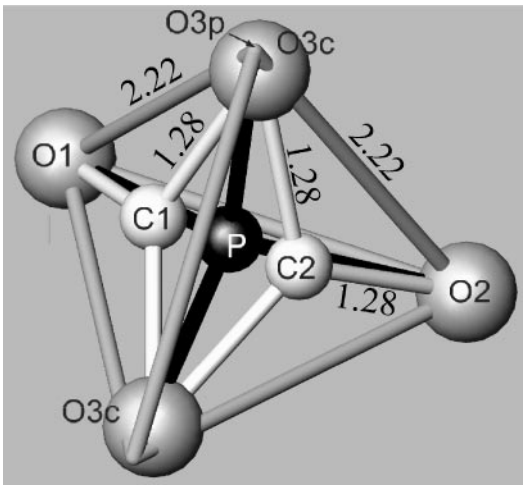


**FIG. 4.** $PO_4$ tetrahedron with $CO_3$ triangles located on its faces. C–O and O–O distances (in ångstroms) are indicated.

$10^{-6}$ and $\Delta c/c = 12.5 \times 10^{-6}$ per °C. The latter value is close to the thermal expansion $\Delta c/c$ of stoichiometric hydroxyapatite, whereas the first one is sufficiently higher than its $\Delta a/a$. This is the consequence of a much higher sensitivity of lattice constant $a$ to the process of decarbonation of the apatite structure. However, the behavior of lattice constant $c$ at elevated temperatures should be also taken into account since it reflects some processes of thermal decomposition, namely, the loss of lattice water and the relocation of carbonate ions.

*Crystal Structure*

Comparing our structural data with the data available in the literature for carbonated and noncarbonated hydroxyapatites (Tables 1, 2) we can conclude that the coordinates of the basic atoms are in good agreement. The greatest discrepancies are found to be in the locations of $O_H$ atoms in the channels, which are quite expected from their well-known positional disorder along the $c$ axis (3, 5, 6). The distinct features of model 1 are the vacancies in Ca1 sites, minor vacancies in two of the three oxygen sites, extra occupation of the sites of $O_H$ in the channels, and high values of their temperature factors (especially along the $z$ axis) as well as shortened P–O3 distances when compared to any of the P–O distances in the structure of Holly Spring hydroxyapatite (13).

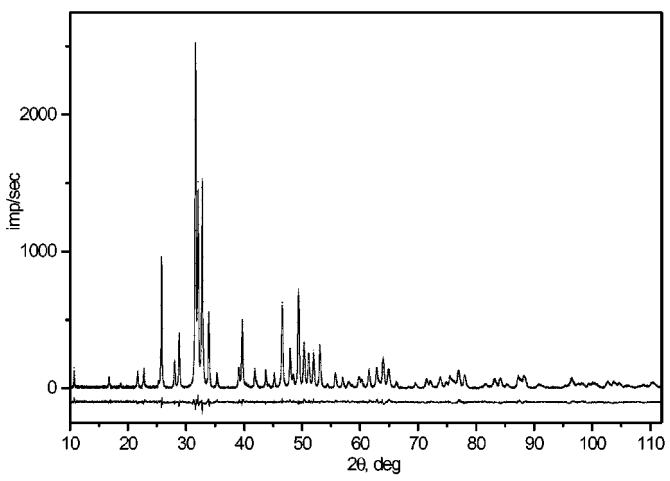


**FIG. 5.** Final fit between experimental (dots) and calculated (line) powder patterns of the sample studied.

The principal difference between the structural models of different natural and synthetic carbonated apatites of B-type including human and animal tooth enamels lies in the distortion modes of $PO_4$ tetrahedra and in the distribution of vacancies between the tetrahedral oxygen sites O1, O2, and O3 (Table 1). It should be noted that there are no concurrent models of several authors. Following the idea of Wilson *et al.* (6), P–O bond length changes seem not to be dominated by replacing $PO_4^{3-}$ by $CO_3^{2-}$ ions, but are also affected by other lattice changes. The structural model of natural francolite suggested by Perdikatsis (4) shows the prominent reduction of P–O1 and P–O2 distances along with vacancies in the O1 and O2 sites, whereas the models proposed by Michel *et al.* (5) for the enamels of modern and fossil red deer both exhibit the diminutions of P–O3 and P–O1 distances, the elongation of P–O2 distances, and the full occupations of all the tetrahedral oxygen sites. The average structural model suggested by Wilson *et al.* (6) for apatites of human tooth enamel is characterized by the significant reduction of only the P–O2 distance but with the vacancies in all of the tetrahedral oxygen sites. However, in the structure of synthetic carbonated apatite refined by the same authors (6) a similar reduction of the P–O2 distance is not accompanied by vacancies in any of the oxygen sites. Our refinement (model 1) of a similar synthetic carbonated apatite with close unit cell constants suggests the shortened P–O3 distances together with some vacancies in the O1 and O2 sites. At the same time the mean P–O distances calculated for all the models show rather good agreement (1.511–1.519 Å) despite the different carbonate contents and occupancies of the phosphorus sites (Table 1). The consideration of the distortions of the $PO_4$ tetrahedra, which are usually taken as evidence for their partial replacement by $CO_3$ groups, does not, however, help much in locating carbonate triangles.

The discrepancies amidst the data of different authors seem to indicate that carbonate triangles may occupy at any of the tetrahedral faces but in each specific case they are found to stick to a certain face(s). As has been already mentioned, it follows from the data of polarized IR spectroscopy (7) that $CO_3$ triangles have their planes oblique to the $c$ axis, making the angle of $37 \pm 4°$ to it and are thought to

occupy the sloping faces of the tetrahedra. Our data (model 2) demonstrate that carbonate ions occupy those two adjacent faces of a $PO_4$ tetrahedron (Fig. 4) which are parallel to the *c* axis. Two orientations of $CO_3$ triangles share one of their edges and are distributed randomly in the structure of carbonated hydroxyapatite, showing their consignificance. Consequently, there are two positions C1 and C2 of carbon atoms with equal occupations of $\sim 0.1$. They are located at the equal distance of 0.6 Å from the position of a phosphorus atom. Each of them has in their coordination one of two oxygen atoms (O1 or O2) that retain their positions in the structure. Two other coordinating oxygen atoms O3c are common for both carbon atoms. O3c atoms are shifted by 0.37 Å from O3p atoms (shown as vertices in Fig. 4) belonging to a $PO_4$ tetrahedron.

The use of model 2 with the split position of O3 atom improved the shape of the $PO_4$ tetrahedron, equalising P–O distances and O–P–O angles and making them somewhat closer to those of non-carbonated apatite (Table 1). However, the P–O3p bond length remained greater than the others. As for C–O distances (1.281–1.283 Å) and O–C–O angles (119.9°–120.1°) in $CO_3$ triangles they are quite similar to those in the structure of calcite (1.287 Å and 120.0°, respectively). Ninefold coordinated Ca1 and sevenfold coordinated Ca2 atoms have distances with oxygen atoms in the range of 2.30–2.83 Å, showing good agreement with calcium polyhedra in the structure of Holly Spring hydroxyapatite (Table 3). Two types of Ca1 and of Ca2 polyhedra are distinguished. Most of them ($\sim 80\%$) include O3p as coordinating oxygen atoms and only 20% include O3c atoms.

It is seen from Table 2 that the sums of the occupational factors of the P, C1, and C2 atoms as well as of the O3p and O3c atoms are close to 1. The sites of the O1 and O2 atoms show some vacancies, whereas the sites of $O_H$ in the channels maintain significantly high occupancy (0.6 instead of 0.5 in stoichiometric hydroxyapatite) and enhanced temperature factors. Both features are typical for the structure of hydroxyapatite and were described earlier by many authors (3–6). The main reasons for that are the positional disorder of OH groups and their partial replacement by water molecules. The charge unbalance occurring when $[CO_3]^{2-}$ ions replace $[PO_4]^{3-}$ groups is primarily compensated by vacancies in the Ca1 sites. The slight diminution of atomic scattering in the Ca2 site is thought to be due to the presence of $(NH_4)^+$ groups.

The unit cell content of the sample $[Ca_{9.3}(NH_4)_{0.1}][P_{4.95}C_{1.05}O_{23.7}][O_{2.4}]$ calculated from the refined occupations of the atomic sites showed satisfactory agreement with the above data on chemical composition but, however, indicated extra oxygen content in the tetrahedra and the channel sites and, consequently, extra negative charge. Accounting for the presence of molecular water in the structure, it was assumed that some part of it occurred in the channels, and another part occupied the vacant oxygen O1 and O2 sites in the $PO_4$ tetrahedra. This assumption was based on the results of STA studies brought in agreement with the X-ray diffraction studies of the sample at the elevated temperatures (Fig. 3). Considering extra oxygen in the form of molecular water and bringing negative and positive charges into balance we come to the final crystallochemical formula of the studied sample of carbonated hydroxyapatite $Ca1_{3.40}[Ca2_{5.90}(NH_4)_{0.10}][(PO_4)_{4.95}(CO_3)_{1.05}(H_2O)_{0.30}][(OH)_{1.65}(H_2O)_{0.45}]$, which gives a total water content of 1.4 wt% close to the value suggested by STA analysis.

**TABLE 3**
**Interatomic Distances (in Å) in the Ca Polyhedra in the Structure of Apatite**

| | Synthetic carbonated hydroxyapatite $Ca_{9.50}(NH_4)_{0.10}(PO_4)_{5.05}(CO_3)_{0.95}(OH)_2$ (our data) model 2 | | Holly Springs hydroxyapatite $Ca_{10}(PO_4)_6(OH)_2$ (13) |
|---|---|---|---|
| Distance | Polyhedron 1 | Polyhedron 2 | |
| Ca1–O1 × 3 | 2.415(3) | 2.415(3) | 2.410 |
| Ca1–O2 × 3 | 2.480(3) | 2.480(3) | 2.456 |
| Ca1–O3p × 3 | 2.826(3) | | 2.809 |
| Ca1–O3c × 3 | | 2.806(3) | |
| Ca2–O1 | 2.648(4) | 2.648(4) | 2.710 |
| Ca2–O2 | 2.331(4) | 2.331(4) | 2.360 |
| Ca2–O3p × 2 | 2.302(3) | | 2.347 |
| Ca2–O3c × 2 | | 2.484(3) | |
| Ca2–O3p × 2 | 2.569(3) | | 2.515 |
| Ca2–O3c × 2 | | 2.801(3) | |
| Ca2–$O_H$ | 2.415(2) | 2.415(2) | 2.387 |

## CONCLUSION

We carried out a full Rietveld refinement on the crystal structure of synthetic carbonated apatite. It was established that carbonate ions randomly occupy the adjacent faces of $PO_4$ tetrahedra, which are parallel to the *c* axis. It was proposed that in general carbonate triangles may occupy any of the tetrahedral faces but in each specific case they are found to stick to a certain face(s). X-ray diffraction and thermogravimetric studies of the sample behavior at elevated temperatures helped to reveal two types of lattice water, which explained extra occupancies of channel and tetrahedral oxygen sites.

## ACKNOWLEDGMENTS

The authors are grateful to Dr. L. G. Poritskaya (St. Petersburg State University) for technical help in the preparation of the sample of carbonated apatite, to Dr. M. L. Zorina (St. Petersburg State University) for the measurement of IR spectrum of the sample, to Mrs. T. N. Kaminskaya (St. Petersburg State University) for the help in performing X-ray diffraction studies at elevated temperatures, and to Dr. Yu. L. Kretser and Mrs. S. N. Zimina (both from Mekhanobr-Analit, St. Petersburg) for the

chemical analysis of the sample. The work was supported by RFBR (Project 98-05-65578).

## REFERENCES

1. M. Mehmel, *Z. Kristallogr.* **75,** 323–331 (1930).
2. A. Ito, S. Nakamura, H. Aoki, M. Akao, K. Teraoka, S. Tsutsumi, K. Onuma, and T. Tateishi, *J. Cryst. Growth* **163,** 311–317 (1996).
3. R. A. Young and P. E. Mackie, *Mater. Res. Bull.* **15,** 17–29 (1980).
4. B. Perdikatsis, *Mater. Sci. Forum* **79–82,** 809–814 (1991).
5. V. Michel, P. Ildefonse, and G. Morin, *Appl. Geochem.* **10,** 145–159 (1995).
6. R. M. Wilson, J. C. Elliott, and S. E. P. Dowker, *Am. Miner.* **84,** 1406–1414 (1999).
7. J. C. Elliott, "Structure and Chemistry of the Apatites and Other Calcium Orthophosphates." Elsevier, Amsterdam (1994).
8. A. B. Koltsov, O. V. Frank-Kamenetskaya, M. L. Zorina, T. N. Kaminskaya, and N. Yu. Vernigora, *Proc. All-Rus. Miner Soc.* **2,** 109–116 (2000). [In Russian]
9. J. C. Trombe and G. Montel, *J. Inorg. Nucl. Chem.* **40,** 15–21 (1978).
10. W. G. Perdok, J. Christoffersen, and J. Arends, *J. Cryst. Growth* **80,** 149–154 (1987).
11. I. A. Kondratyeva and S. K. Filatov, *in* "Proc. XI All-Union Conf. on X-Ray Diffraction of Raw Miner," p. 145. Sverdlovsk (1989). [in Russian]
12. B. Hunter, *IUCr CPD Newsletter* **20,** 21 (1998).
13. K. Sudarsanan and R. A. Young, *Acta Crystallogr. B* **25,** 1534–1543 (1969).
14. E. N. Maslen, V. A. Streltsov, and N. R. Streltsova, *Acta Crystallogr. B* **49,** 636–641 (1993).